frontiers | Frontiers in Earth Science

TYPE Original Research
PUBLISHED 01 September 2023
DOI 10.3389/feart.2023.1257219

OPEN ACCESS

EDITED BY
Hu Li,
Southwest Petroleum University, China

REVIEWED BY
Hong-Bin Liang,
Chongqing University of Science and Technology, China
Lingfu Liu,
University of Wyoming, United States

*CORRESPONDENCE
Keren Wang,
wangkeren@petrochina.com.cn

RECEIVED 12 July 2023
ACCEPTED 21 August 2023
PUBLISHED 01 September 2023

CITATION
Xiao H, Chen M, Jing C, Zhao H and Wang K (2023), Production simulation and prediction of fractured horizontal well with complex fracture network in shale gas reservoir based on unstructured grid.
Front. Earth Sci. 11:1257219.
doi: 10.3389/feart.2023.1257219

Production simulation and prediction of fractured horizontal well with complex fracture network in shale gas reservoir based on unstructured grid

Hongsha Xiao[1], Man Chen[1], Cui Jing[1], Huiyan Zhao[1] and Keren Wang[2]*

[1]Sichuan Changning Natural Gas Development Co., Ltd., Chengdu, Sichuan, China, [2]Development Division of Southwest Oil & Gas Field Company, Chengdu, Sichuan, China

In order to accurately simulate the productivity variation characteristics of fractured wells with complex fracture network in shale gas reservoir, based on the multiple migration mechanism of shale gas, the micro-seismic data and discrete fracture model were used to characterize the fracture geometry and complex boundary characteristics, and the comprehensive seepage mathematical model of fractured wells with complex fracture network was established based on the dual porosity-discrete fracture model, and the numerical solution was carried out by combining the unstructured grid and the control volume finite element method. The sensitivity analysis of the influence of key parameters such as fracture conductivity, physical property difference in composite area and Langmuir volume on the production performance of fractured horizontal wells is carried out. This study provides theoretical methods and calculation tools for accurate prediction of productivity change and optimization of production system of fractured horizontal wells with complex fracture network in shale gas reservoirs.

KEYWORDS

shale gas reservoir, complex fracture network, fractured horizontal well, production prediction, numerical simulation

1 Introduction

Shale gas reservoir is an important exploration field proposed in China's energy development plan to vigorously enhance exploration and development, and continuously and efficiently promote the development and utilization of shale gas resources, which has important strategic significance for optimizing China's clean energy production capacity layout and reducing natural gas dependence on foreign countries (Zou et al., 2020). China is generally rich in shale gas resources. It is estimated that the technically recoverable reserves of shale gas in China are 21.8 trillion cubic meters, and the proven reserves exceed 1 trillion cubic meters (Li, 2023). At present, three national shale gas demonstration zones have been built in Fuling, Changning-Weiyuan and Zhaotong, and China's shale gas production is planned to reach 80 to 100 billion cubic meters by 2030 (Yang et al., 2020).

By referring to the key technologies of the shale gas revolution in North America, the multi-cluster fracturing technology of horizontal wells has become a key method to efficiently develop and utilize shale gas resources (Wu et al., 2022; Sun, 2023). Through

the implementation of the "close cutting and large displacement and temporary plugging and diversion" technology, the tight reservoir is "broken" to form the SRV (stimulated reservoir volume) region, the natural fracture groups around the near well are opened and communicated, the seepage field around the horizontal wellbore is improved, and the final recoverable reserves of a single well are increased (Xie, 2018; Liu et al., 2019). However, the characterization of complex fracture network geometry and mathematical expression of flow exchange between different systems have been the key problems, affecting prediction accuracy of production after fracturing. Brown et al. (2011), Yuan et al. (2015) divided the fractured horizontal well and shale gas reservoir into stimulated and initial regions, adopting multi-linear and dual porosity models to obtain the solution. Xu et al. (2015), Fan et al. (2015), Zhang et al. (2015) respectively used the circular or rectangular composite region model to simplify the complex fracture geometry, and the flow characterization was carried out by combining the continuum model. In order to more accurately predict the effect of fracture properties on flow mechanism and production, Karimi-Fard et al. (2004), Altwaijri et al. (2018) established the discrete fracture model to display and characterize the length, angle and width of each fracture, and then carried out the production impact analysis. Jiang and Rami (2015) further combined the respective advantages of continuous medium model and discrete fracture model, the discrete fracture model is adopted for large-scale hydraulic fracturing fractures, and continuous medium model is used for small-scale natural fracture system, which ensures the efficiency and accuracy of production prediction of fractured horizontal wells with complex fractures. However, the above models did not take into account the gas-water two-phase flow in the SRV region and gas-water co production characteristics caused by fracturing fluid retention.

In addition, researchers (Ozkan et al., 2011; Stalgorova and Mattar, 2013; Wang, 2014; Li et al., 2015; Zhao et al., 2018) established analytical and semi-analytical models respectively to predict the production of horizontal wells after fracturing in shale gas reservoirs. However, the analytical and semi-analytical model mainly uses the symmetric main fracture model, the whole or local regular rectangular or circular SRV region to simplify the hydraulic fracture network, and for gas-water two-phase flow, an approximate solution is obtained by defining a pseudo pressure function to transform it into single-phase seepage. The above processing will significantly affect the accuracy of production performance and productivity prediction for fractured horizontal wells. The numerical model is more suitable to deal with the geometry characteristics of the complex fracture network, and can accurately characterize the complex boundary characteristics of the fracture network through the spatial mesh dispersion, and is convenient for coupling the multi-scale and multi-phase seepage mechanism of shale gas reservoirs (Wu and Pruess, 1988; Geiger et al., 2004; Lv et al., 2012; Moinfar et al., 2013; Wu, 2014; Zhang et al., 2017; Wang et al., 2020; Zhang et al., 2023).

To sum up, this study combined with micro-seismic data and discrete fracture model to characterize fracture geometry and complex boundary characteristics on the basis of comprehensive consideration of multiple flow mechanisms in shale gas reservoir, and established a dual continuum-discrete fracture coupling seepage model. A fully implicit numerical solution model is established by using unstructured triangular mesh and controlled volume finite element method. Combined with the field data, the productivity change characteristics of horizontal wells after fracturing were simulated and predicted, and the key factors affecting the production and EUR of single well were analyzed.

2 Physical model and basic assumptions

Natural fractures and bedding are developed in shale reservoirs, the brittle mineral content of favorable development series of strata is high (Cai, 2020; Zhu et al., 2022; Li et al., 2023), and the fracture network stimulation area is formed near the well after fracturing (Zhao et al., 2018). The field monitoring of micro-seismic results of shale fractured horizontal wells shows (as shown in Figure 1) that there are dense signal response points around the wellbore during the fracturing process, and complex reformations are formed during the fracturing process. Therefore, micro-seismic monitoring data and discrete fracture model were applied to characterize the fracture geometry and complex boundary characteristics of the reconstruction area, and the flow characteristics of the composite area of the original reservoir and the stimulation area were described based on the dual medium model (Moinfar et al., 2013; Cheng et al., 2020).

The assumptions of the physical model are as follows: 1) Considering the retention of fracturing fluid in the formation, gas-water two-phase flow occurs in hydraulic fracturing fractures and fractures in the reconstruction area, while single-phase gas isothermal seepage occurs in the shale matrix and the original reservoir area. 2) Ignoring the vertical heterogeneity of physical properties of shale reservoirs, two-dimensional grid is used to describe them approximately; 3) There is a quasi steady state channeling between the matrix system and the fracture system, and the fluid enters the fracture system from the matrix system under the action of pressure difference, and flows into the horizontal wellbore through the fracture and produces.

3 Mathematical model

3.1 Micro-nano scale flow model of shale gas reservoir

Shale reservoir has a complex pore structure, and gas seepage in the reservoir has multiple flow mechanisms such as Knudsen diffusion, surface adsorption diffusion, slip flow and viscous flow (Geng et al., 2016; Wu et al., 2016; Zhang et al., 2018) (as shown in Figure 2).

In the process of shale gas development, the thickness of adsorption layer decreases, and the effective flow pore size increases further. The effective pore radius of removing the adsorption layer can be expressed as:

$$r_{abs} = r - d_M\theta = r - d_M\frac{p/Z}{p/Z + p_L} \tag{1}$$

Where, d_M is the molecular diameter of the gas, m; r is the actual radius of the matrix pores, m; θ is the true gas coverage, dimensionless; p is the current pore pressure, Pa; p_L is Langmuir pressure, Pa; Z is the true gas compression factor, dimensionless.

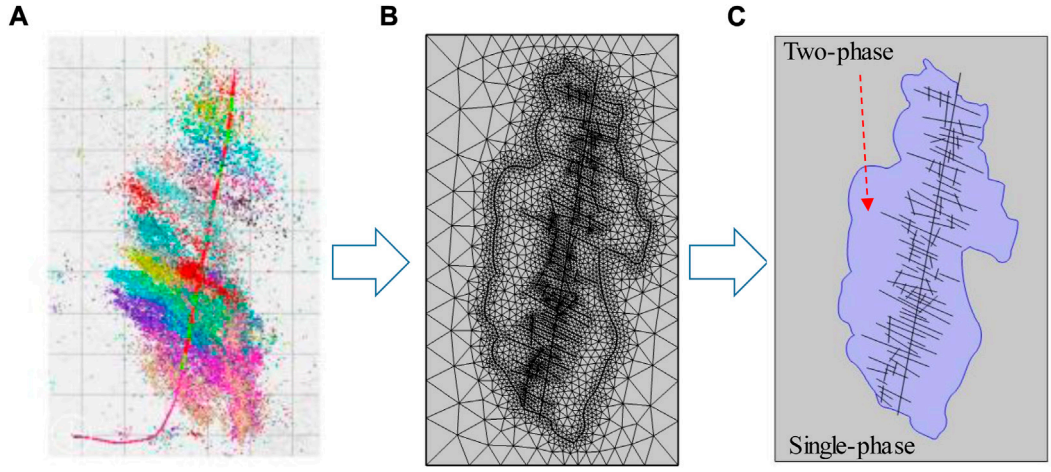

FIGURE 1
Diagram of physical model. **(A)** Model of fractured horizontal well with complex fracture network in shale gas reservoir based on micro-seismic data (Cheng et al., 2020). **(B)** Schematic diagram of grid division (6,857 triangles). **(C)** Assumptions of seepage models in different regions.

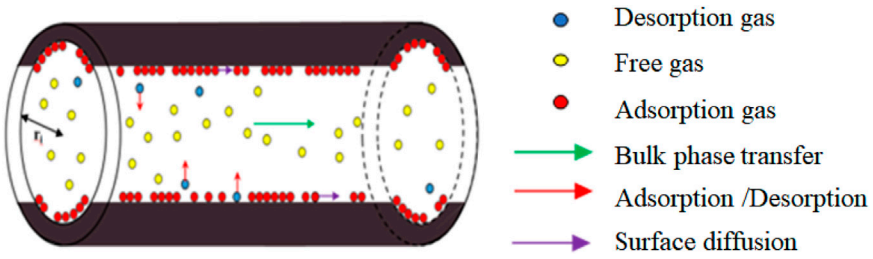

FIGURE 2
Gas transport mechanism in micro and nano pores of shale matrix (Javadpour, 2009; Guo et al., 2022).

Considering the stress-sensitive effect, the porosity and permeability of shale matrix related to pore pressure can be expressed as:

$$\begin{aligned}\varphi(p) &= \varphi_r + (\varphi_i - \varphi_r)e^{-\eta(p_i-p)}\\ k(p) &= k_i e^{-\Psi(p_i-p)}\end{aligned} \tag{2}$$

Where, $\varphi(p)$ is the porosity of the matrix considering stress sensitivity; φ_i is the initial porosity, dimensionless; φ_r is the porosity under maximum stress, dimensionless. $k(p)$ is the matrix permeability after considering stress sensitivity, nD; k_i is the original permeability of matrix, nD; η is the stress sensitivity coefficient of porosity, Pa^{-1}; ψ is the stress-sensitive coefficient of permeability, Pa^{-1}; p_i is the original gas reservoir pressure, Pa.

The effective pore radius of the matrix considering the thickness of the adsorption layer and the stress-sensitive effect is as follows:

$$r_e = \sqrt{8\tau \frac{k_{on,abs}e^{-\Psi(p_i-p)}}{\varphi_r + (\varphi_i - \varphi_r)e^{-\eta(p_i-p)}}} \tag{3}$$

Where, τ is the tortuosity, which is the ratio of the actual length of the flow path to the represented length.

In the circular organic nanopores, the apparent permeability contributed by the bulk phase gas based on the Beskok model can be expressed as:

$$k_{\text{on,bulk}} = -\frac{r_e^2\varphi(p)}{8\tau}(1+\alpha Kn)\left(1+\frac{4Kn}{1+Kn}\right) \tag{4}$$

Where, Kn is Knudsen diffusion constant, dimensionless; α is the rarefied gas effect coefficient, dimensionless, which can be calculated by the following equation:

$$\alpha = \alpha_0\frac{2}{\pi}\tan^{-1}\left(\alpha_1 Kn^{\beta}\right) \tag{5}$$

Where, α_0 is the rarefied gas coefficient under $K_n\rightarrow\infty$ condition; α_1 and β are fitting constants.

The apparent permeability considering the real gas effect can be expressed as:

$$k_{\text{on,surface}} = D_s\frac{\mu_{gr}RTC_{sc}\varphi(p)}{M_g p^2\tau} \tag{6}$$

Where, D_s is the surface diffusion coefficient, m^2/s; μ_{gr} is the gas viscosity after considering the real gas effect, mPa·s; R is the universal gas constant, Pa/(mol•K); T is the absolute

temperature, K; M_g is the molecular weight of gas, g/mol; C_{sc} is the concentration of adsorbed gas in Langmuir monolayer on the pore surface, kg/m^3. The calculation equation is as follows:

$$C_{sc} = \frac{4\theta M_g}{\pi d_M^3 N_A} \tag{7}$$

Where, N_A is Avogadro's constant, 6.022×10^{23}mol^{-1}.

The surface diffusion coefficient can be calculated as follows:

$$D_s = D_s^0 \frac{(1-\theta) + \frac{\kappa}{2}\theta(2-\theta) + [H(1-\kappa)](1-\kappa)\frac{\kappa}{2}\theta^2}{\left(1-\theta+\frac{\kappa}{2}\theta\right)^2} \tag{8}$$

$$H(1-\kappa) = \begin{cases} 0, \kappa \geq 1 \\ 1, 0 \leq \kappa \leq 1 \end{cases}, \kappa = \frac{\kappa_b}{\kappa_m} \tag{9}$$

Where, $H(1\text{-}\kappa)$ is Heaviside function; κ_b is the plugging rate, m/s; κ_m is migration rate, m/s; D_s^0 represents the surface diffusion coefficient when the gas coverage is 0, m^2/s, which is calculated by the following equation:

$$D_S^0 = 8.29 \times 10^{-7} T^{0.5} e^{-\frac{\Delta H^{0.8}}{RT}} \tag{10}$$

Where, ΔH is the isothermal adsorption heat of gas, J/mol.

The total gas transport flux includes free gas phase transport and surface diffusion of adsorbed gas in circular tube pores. After taking into account the cross-sectional area of the circular tube, the apparent permeability of the matrix pore is as follows:

$$\begin{aligned} k_{app} &= \varsigma_{bulk} k_{on,bulk} + \varsigma_{surface} k_{on,surface} \\ &= \frac{r_e^2}{(r_e^2 + \theta d_M)} k_{on,bulk} + \left[1 - \frac{r_e^2}{(r_e^2 + \theta d_M)}\right] k_{on,surface} \end{aligned} \tag{11}$$

Where ς_{bulk} is body phase gas weight coefficient, its value is equal to the ratio of the cross-sectional area occupied by the body phase gas and the total cross-sectional area, dimensionless; $\varsigma_{surface}$ is surface diffusion weight coefficient, its value is equal to the ratio of the cross-sectional area occupied by the surface diffusion gas to the total cross-sectional area, dimensionless.

3.2 Comprehensive seepage model of multi-scale flow mechanisms

Further, based on the dual media-discrete fracture model, the comprehensive seepage model of fractured horizontal well is established as follows:

①Seepage control equations of matrix system:

$$\nabla \cdot \left(\frac{k_{app}}{\mu_g B_g} \nabla p_{gml}\right) - \alpha_l \frac{k_{app}}{\mu_g B_g}\left(p_{gml} - p_{gfl}\right) + q_{des} = \frac{\partial\left(\phi_{ml}/B_g\right)}{\partial t} \tag{12}$$

Where,

$$q_{des} = -\rho_s\left(1 - \phi_{ml} - \phi_{fl}\right)\frac{\partial V_E}{\partial t} \tag{13}$$

Where, B_g is the volume coefficient of gas, dimensionless; p_{gm} is the matrix system gas pressure, MPa; p_{gf} is the fracture system gas pressure, MPa; q_{des} is the desorption production of matrix, m^3/s; φ_m is the matrix system porosity, dimensionless; φ_f is the porosity of fracture system, dimensionless; α is the shape factor, dimensionless; ρ_s is the density of shale rock, g/cm^3; The subscripts l=1, 2, 1 denotes the inner zone, 2 denotes the outer zone.

②Seepage control equations of fracture system:

For inner zone:

$$\nabla \cdot \left(\frac{k_f k_{ru1}}{\mu_u B_u} \nabla p_{fu1}\right) + \alpha_1 \frac{k_{app} k_{ru1}}{\mu_u B_u}\left(p_{mu1} - p_{fu1}\right) = \frac{\partial}{\partial t}\left(\frac{S_{fu1}\phi_{f1}}{B_u}\right) \tag{14}$$

For outer zone:

$$\nabla \cdot \left(\frac{k_f}{\mu_g B_g} \nabla p_{fg2}\right) + \alpha_2 \frac{k_{app}}{\mu_g B_g}\left(p_{mg2} - p_{fg2}\right) = \frac{\partial}{\partial t}\left(\frac{\phi_{f2}}{B_g}\right) \tag{15}$$

Where, p_f is the pressure of the natural fracture system, MPa; k_f is the permeability of natural fractures in shale reservoirs, mD; k_r is the relative permeability, dimensionless; Subscript u=g, w, where g represents the gas phase and w represents the water phase.

③Control equations of hydraulic fracture seepage:

$$\nabla \cdot \left(\frac{k_F k_{rul}}{\mu_u B_u} \nabla p_{Fu}\right) + q_{usct} = \frac{\partial}{\partial t}\left(\frac{\phi_F S_{Fu}}{B_u}\right) \tag{16}$$

Where, k_F is hydraulic fracture permeability, mD; φ_F is the hydraulic fracture porosity, dimensionless; q_{gsct} is horizontal well production, m^3/s; p_F is the hydraulic fracture pressure, MPa.

4 Model solving

4.1 Element characteristic matrix

First, the element characteristic matrix of Eq. (12) is constructed based on triangular mesh and control volume finite element method (as shown in Figure 3), and the average mesh pressure p_{gm} and average saturation S_{fu} of the matrix system are approximated by triangle vertex interpolation:

$$\begin{aligned} p_{gm}(x,y) &= \sum_{v=i}^{k} N_v(x,y) p_{gmv}, p_{ful}(x,y) = \sum_{v=i}^{k} N_v(x,y) p_{fulv} \\ S_{ful}(x,y) &= \sum_{v=i}^{k} N_v(x,y) S_{fulv} \end{aligned} \tag{17}$$

Where N_v is the interpolation function.

For the convection term in the matrix system seepage equations, Galerkin's weighted margin method and Gauss's law are used to obtain:

$$\iint_{\Omega_i} \nabla \cdot \left(\bar{\bar{\lambda}} \cdot \nabla p_{gml}\right) dV = \sum_{v=j,k} T_{iv}\left(p_{igml} - p_{vgml}\right) \tag{18}$$

Where T_{iv} represents the conductivity matrix given by the following equation:

$$\begin{aligned} T_{iv} &= A\left(\lambda_x \frac{\partial N_i}{\partial x}\frac{\partial N_v}{\partial x} + \lambda_y \frac{\partial N_i}{\partial y}\frac{\partial N_v}{\partial y}\right) \\ &= \frac{1}{4A}\left(\lambda_x a_i a_l + \lambda_y b_i b_l\right) \end{aligned} \tag{19}$$

The above equations establish the net flow of the control volume of the inflow node i of triangle ijk. Similarly, the net inflow flow equation of nodes j and k can be established. Then the flow matrix of the virtual finite control volume unit can be obtained as:

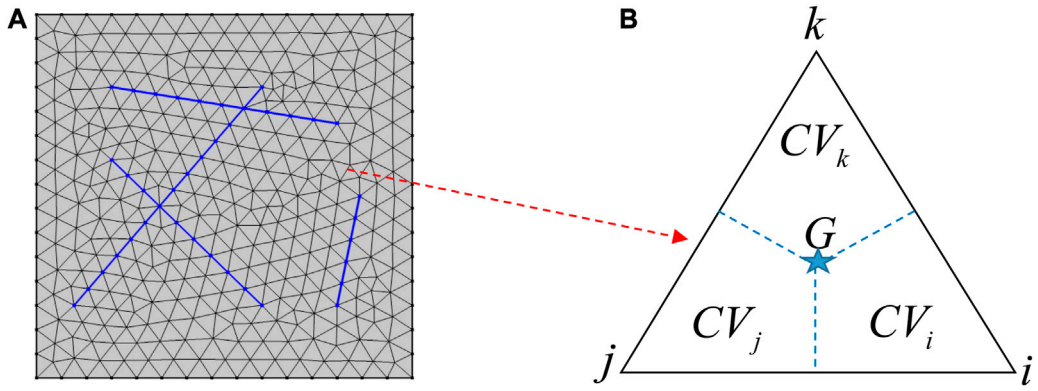

FIGURE 3
Schematic diagram of unstructured mesh generation. **(A)** Triangular mesh generation for large-scale discrete fractures. **(B)** Virtual finite control volume mesh in triangular mesh, which is formed by connecting the center of gravity of a triangle to the midpoint of each side.

$$\begin{pmatrix} T_{ij}+T_{ik} & -T_{ij} & -T_{ik} \\ -T_{ji} & T_{ji}+T_{jk} & -T_{jk} \\ -T_{ki} & -T_{kj} & T_{ki}+T_{kj} \end{pmatrix} \begin{pmatrix} p_{igml} \\ p_{jgml} \\ p_{kgml} \end{pmatrix} = \begin{pmatrix} f_{gmi} \\ f_{gmj} \\ f_{gmk} \end{pmatrix} \tag{20}$$

Eq. (20) is the processing format of the convection term of the controlled volume finite element method based on triangular mesh. In Eq. (12), the cross-flow term between matrix system and fracture system, as well as the adsorption and desorption term and the time derivative term of matrix system are numerically calculated using the traditional finite element method.

Taking gas phase as an example, the finite element integral numerical calculation format for constructing the cross-flow term is as follows:

$$\begin{aligned} \iint_{\Omega_m} N_v \alpha \frac{k_{app}}{\mu_g B_g}(p_m - p_f) d\Omega_m &= \iint_{\Omega_m} N_v \alpha \frac{k_{app}}{\mu_g B_g}\left(\sum_{v=i}^{k} N_v p_{mv} - \sum_{v=i}^{k} N_v p_{fv}\right) d\Omega_m \\ &= \begin{pmatrix} \left(\alpha \frac{Ak_{app}}{3\mu_g B_g}\right)_i & 0 & 0 \\ 0 & \left(\alpha \frac{Ak_{app}}{3\mu_g B_g}\right)_j & 0 \\ 0 & 0 & \left(\alpha \frac{Ak_{app}}{3\mu_g B_g}\right)_k \end{pmatrix} \begin{pmatrix} p_{mi} - p_{fi} \\ p_{mj} - p_{fj} \\ p_{mk} - p_{fk} \end{pmatrix} \end{aligned} \tag{21}$$

For the adsorption and desorption term and the time derivative term, the finite element integral numerical calculation format is constructed by combining Euler backward difference as follows:

$$\begin{aligned} &\frac{A}{3\Delta t}\begin{pmatrix} \left(\frac{\phi_m}{B_g}\right)_i^{n+1} - \left(\frac{\phi_m}{B_g}\right)_i^{n} \\ \left(\frac{\phi_m}{B_g}\right)_j^{n+1} - \left(\frac{\phi_m}{B_g}\right)_j^{n} \\ \left(\frac{\phi_m}{B_g}\right)_k^{n+1} - \left(\frac{\phi_m}{B_g}\right)_k^{n} \end{pmatrix} \\ &+ \frac{A}{3\Delta t}\begin{pmatrix} [(1-\phi_m-\phi_f)V_E]_i^{n+1} - [(1-\phi_m-\phi_f)V_E]_i^{n} \\ [(1-\phi_m-\phi_f)V_E]_j^{n+1} - [(1-\phi_m-\phi_f)V_E]_j^{n} \\ [(1-\phi_m-\phi_f)V_E]_k^{n+1} - [(1-\phi_m-\phi_f)V_E]_k^{n} \end{pmatrix} \end{aligned} \tag{22}$$

Eqs 17–22 construct the element characteristic matrix of shale matrix gas phase seepage equation based on triangular mesh and controlled volume finite element method. Similarly, the element characteristic matrix of shale fracture system seepage equation can be constructed.

For hydraulic fracturing fractures, the discrete fracture model is used to reduce their dimensionality to a one-dimensional line segment with a certain width. The interpolation function of the gas phase equation can be expressed as:

$$\begin{aligned} p_{gF} &= \frac{x_j - x}{\Delta l} p_{gFi} + \frac{x - x_i}{\Delta l} p_{gFj} \\ &= N_i p_{gFi} + N_j p_{gFj} \\ &= \begin{bmatrix} N_i & N_j \end{bmatrix} \begin{bmatrix} p_{gFi} \\ p_{gFj} \end{bmatrix} \end{aligned} \tag{23}$$

Combined with the interpolation function, Eq. (16) of the hydraulic fracture seepage control equation is constructed in the following numerical calculation format:

$$\begin{aligned} &\iint_{\Omega_F} N_v \frac{\partial}{\partial l_F}\left(\lambda_{gF} \frac{\partial p_{gF}}{\partial l_F}\right) d\Omega_F \\ &= w_F \times \Delta l_F \times \lambda_{gF} \times \frac{\partial N_v}{\partial l_F}\begin{bmatrix} \frac{\partial N_i}{\partial l_F} & \frac{\partial N_j}{\partial l_F} \end{bmatrix} \begin{bmatrix} p_{gFi} \\ p_{gFj} \end{bmatrix} \\ &= w_F \times \lambda_{gF} \times \begin{bmatrix} \frac{1}{\Delta l_F} & -\frac{1}{\Delta l_F} \\ -\frac{1}{\Delta l_F} & \frac{1}{\Delta l_F} \end{bmatrix} \begin{bmatrix} p_{gFi} \\ p_{gFj} \end{bmatrix} \end{aligned} \tag{24}$$

For the time term:

$$\iint_{\Omega_F} N_l \frac{\partial\left(S_{gF}\phi_F / B_{gF}\right)}{\partial t} d\Omega_F = w_F \times \frac{\Delta l_F}{2\Delta t} \times \begin{pmatrix} \left(\frac{S_{gF}\phi_F}{B_{gF}}\right)_i^{n+1} - \left(\frac{S_{gF}\phi_F}{B_{gF}}\right)_i^{n} \\ \left(\frac{S_{gF}\phi_F}{B_{gF}}\right)_j^{n+1} - \left(\frac{S_{gF}\phi_F}{B_{gF}}\right)_j^{n} \end{pmatrix} \tag{25}$$

Similarly, the characteristic matrix of water phase unit in fracturing fracture system can be further constructed.

4.2 The whole region iteratively solves the matrix

The pressure value of each system in the next time step is characterized by the fully implicit calculation format. The "dimensionality reduction" treatment of fractured fractures is carried out and embedded into the reservoir flow model. By assembling the characteristic matrix of each unit, the fully implicit iterative solution matrix for the whole region is constructed as follows:

$$\begin{Bmatrix} \mathbf{T}_{\mathrm{gf}}^{k}+\delta\mathbf{T}_{\mathrm{gf}}^{k}\mathbf{P}_{\mathrm{gf}}^{k}-\mathbf{W}_{\mathrm{gmf}}^{k}-\dfrac{\delta\mathbf{N}_{\mathrm{gf}}^{k}}{\Delta t} & \delta\mathbf{W}_{\mathrm{gmf}}^{k}\left(\mathbf{P}_{\mathrm{gm}}^{k}-\mathbf{P}_{\mathrm{gf}}^{k}\right)+\mathbf{W}_{\mathrm{gmf}}^{k} & \delta\mathbf{T}_{\mathrm{gf}}^{k}\mathbf{P}_{\mathrm{gf}}^{k}+\dfrac{\delta\mathbf{N}_{\mathrm{gf-S_{wf}}}^{k}}{\Delta t} \\ \mathbf{W}_{\mathrm{gmf}}^{k} & \mathbf{T}_{\mathrm{gm}}^{k}+\delta\mathbf{T}_{\mathrm{gm}}^{k}-\delta\mathbf{W}_{\mathrm{gmf}}^{k}\left(\mathbf{P}_{\mathrm{gm}}^{k}-\mathbf{P}_{\mathrm{gf}}^{k}\right) & \\ & -\mathbf{W}_{\mathrm{gmf}}^{k}-\dfrac{\delta\mathbf{N}_{\mathrm{gm}}^{k}}{\Delta t}-\dfrac{\delta\mathbf{V}^{k}}{\Delta t} & \\ \mathbf{T}_{\mathrm{wf}}^{k} & & \delta\mathbf{T}_{\mathrm{gf}}^{k}\mathbf{P}_{\mathrm{gf}}^{k}+\dfrac{\delta\mathbf{N}_{\mathrm{wf}}^{k}}{\Delta t} \end{Bmatrix} \times \begin{bmatrix} \delta\mathbf{P}_{\mathrm{gf}}^{k} \\ \delta\mathbf{P}_{\mathrm{gm}}^{k} \\ \delta\mathbf{S}_{\mathrm{wf}}^{k} \end{bmatrix} = \begin{bmatrix} \mathbf{R}_{\mathrm{gf}}^{k} \\ \mathbf{R}_{\mathrm{gm}}^{k} \\ \mathbf{R}_{\mathrm{wf}}^{k} \end{bmatrix} \tag{26}$$

Finally, the numerical well model of fractured horizontal well is established and put into Eq. (26):

$$q_{u\mathrm{sct}}^{n+1}=\sum_{i=1}^{N_F}\mathrm{PI}_{ui}^{n+1}\left(p_{\mathrm{bh}}-p_{\mathrm{avei}}\right)^{n+1} \tag{27}$$

Where, $q_{u\mathrm{sct}}$ is the daily gas and water production ground conditions, m^3/d; p_{bh} is bottom-hole flow pressure, MPa; p_{avei} is the average pressure of the grid block where the well source and junction are located, MPa; N_F is the total number of intersection points between fractured fractures and horizontal wellbore. PI_{ui} is the production index, $m^3/d/MPa$. Through iterative computations, when the accuracy requirements of δP and δS_w are met, the stable value under current time step is obtained and the calculation of the next time step is started.

5 Results and discussion

5.1 Pressure distribution prediction and analysis

For a fractured horizontal well with a complex fracture network (Figure 1) in the south Sichuan shale gas reservoir block, the triangular grid was used to discrete the spatial grid of the whole area, and a fully implicit numerical simulation program was developed to simulate and predict the production dynamic characteristics of fractured horizontal wells. The basic parameters of the model are shown in Table 1. The calculation equation of the fracture relative permeability curve is: k_{rgf}=1-S_{wf}, k_{rwf}=S_{wf}.

Figure 4 shows the change of gas well pressure of fractured horizontal wells with complex fracture networks of shale gas for 100 days, 1 year and 10 years, respectively. As can be seen from the figure, the pressure propagation presents the characteristics of non-uniform distribution in the complex fracture network area, and the pressure propagation is faster in the well section with high reconstruction degree. At the same time, the gas well pressure propagation gradually expands outward with time, and the pressure at the boundary of the inner and outer regions is also non-uniform due to the influence of the complex fracture network boundary shape. When the pressure propagates to the original reservoir area, its pressure propagation speed is significantly slower than that of the reconstruction area, indicating that the reconstruction area of complex fracture network is the main contribution area to the pressure drop and production of shale gas wells.

In addition, Figure 5 shows the production decline curves of fractured horizontal wells with and without SRV region. By comparison, it can be seen that the SRV region formed by complex fracture networks will significantly increase the daily and cumulative gas production of fractured wells, indicating that compared to traditional double wing hydraulic fracturing method, fracture network fracturing is more conducive to achieving higher single well EUR and production efficiency for horizontal wells in shale gas reservoirs.

5.2 Effect of fracture water saturation on productivity

Figure 6 shows the influence of different fracture water saturation on gas well productivity. Due to the low flowback rate of fracturing fluid in shale reservoirs, a large amount of fracturing fluid remains in the reservoir, resulting in gas-water two-phase flow characteristics in fractured wells and near wellbores. The simulation results show that the higher the fracture water saturation, the lower the daily gas production. When the fracture water saturation is 0.2, 0.3, and 0.4, the cumulative gas production after 10 years of depletion production is 194 million m^3, 170 million $m^3$and 145 million m^3, respectively. Therefore, the retained fracturing fluid has a significant impact on gas well productivity.

5.3 Effect of fracture conductivity on productivity

Figure 7 shows the influence of different hydraulic fracture conductivity on gas well productivity. As can be seen from the figure, the higher the diversion capacity, the higher the early daily gas output, but the difference degree gradually decreases with the increase of production time. When the diversion capacity CFD is 0.25D cm, 0.5D cm and 1.0D cm, the cumulative gas production after 10 years of depletion is 133 million m^3, 180 million m^3 and 194 million m^3, respectively. Therefore, in the hydraulic fracturing process of shale gas reservoir, it is necessary to improve the conductivity of fracturing fractures as much as possible to increase the production.

5.4 Effect of permeability of stimulation area on productivity

Figure 8 shows the influence of permeability in the stimulation area on gas well productivity. It can be seen that the higher the permeability of the stimulation area, the larger the daily gas

TABLE 1 Basic parameters of the model.

Original reservoir pressure, p_i, MPa	46	Matrix nanopore radius, r_e, nm	2
Reservoir thickness, h, m	80	Stress sensitivity factor, d_f, MPa^{-1}	0.05
Horizontal well length, L, m	1700	Reservoir temperature, T, K	323
Bottom hole flow pressure, p_{bh}, MPa	14	gas specific gravity, r_g	0.6
Langmuir pressure, p_L, MPa	15	Langmuir volume, V_L, m^3/kg	0.01
Stimulated inner zone		**Outer zone**	
Fracture permeability, k_{f1}, mD	0.001	Fracture permeability, k_{f2}, mD	0.0005
Fracture porosity, φ_{f1}	0.15	Fracture porosity, φ_{f2}	0.05
Matrix permeability, k_{m1}, mD	0.0001	Matrix permeability, k_{m2}, mD	0.0001
Matrix porosity, φ_{m1}	0.02	Matrix porosity, φ_{m2}	0.02
Fracture water saturation, S_{wf1}	0.2	Fracture water saturation, S_{wf2}	0

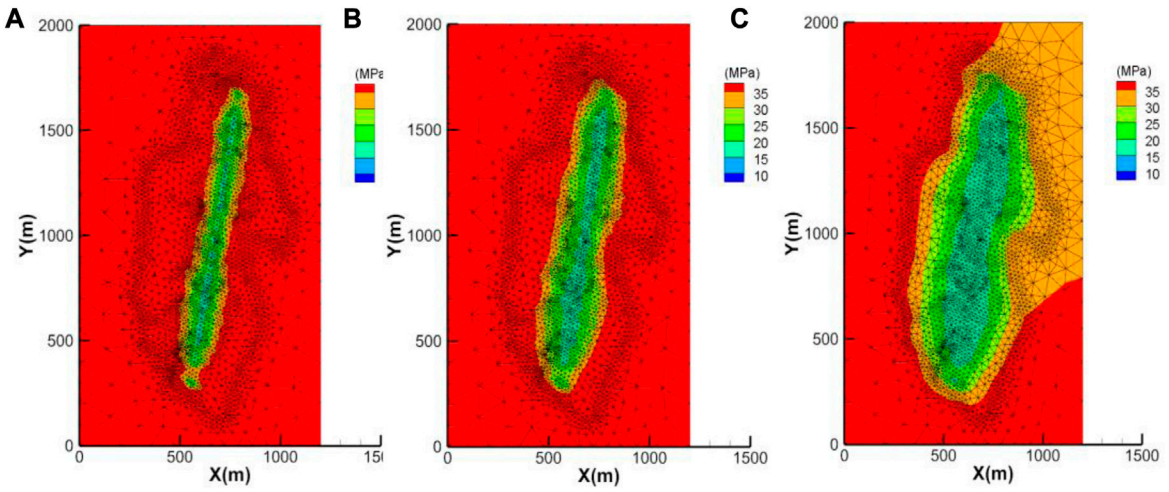

FIGURE 4
Pressure distribution of fractured wells with complex fracture network under different production time. **(A)** After 100 days' production. **(B)** After 1 year' production. **(C)** After 10 years' production.

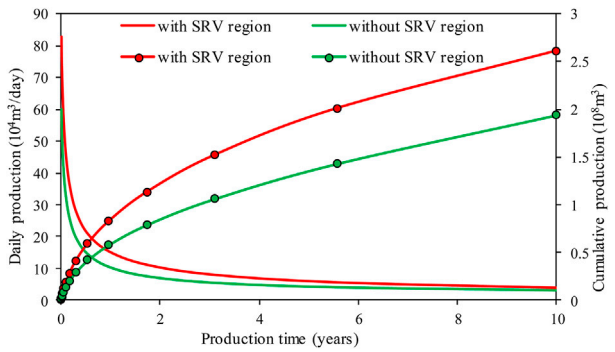

FIGURE 5
Production of fractured horizontal well with and without SRV region.

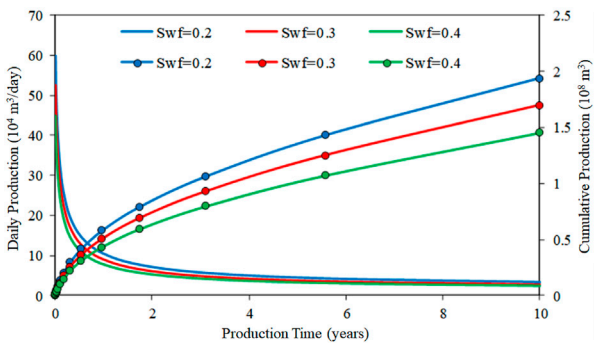

FIGURE 6
Effect of different fracture water saturation on gas well production.

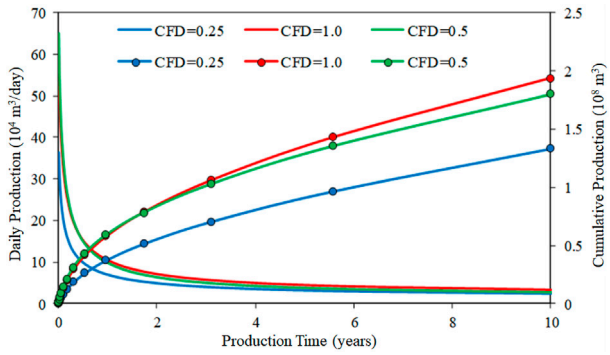

FIGURE 7
Effect of different fracture conductivity on gas well production.

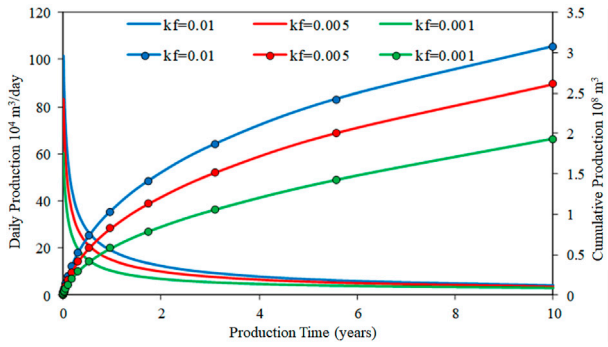

FIGURE 8
Effect of different permeability in SRV region on gas well production.

production of the gas well in the early stage, and the larger the cumulative production of the gas well, indicating that the fracturing stimulation area around the horizontal well is more fully stimulated. When the fracture permeability in the stimulation area is 0.001mD, 0.005mD and 0.01mD, the cumulative gas production after 10 years of depletion production is 194 million m^3, 261 million m^3 and 308 million m^3, respectively. It is the key to improve the production of shale gas wells by optimizing the construction parameters, increasing the stimulation degree of the stimulation area and improving the seepage capacity of shale reservoir.

5.5 Effect of Langmuir volume on productivity

Figure 9 shows the influence of different Langmuir volume V_L on gas well production curves. As can be seen from the figure, the larger the V_L value, the larger the daily gas production and cumulative gas production of the gas well, and the slower the decline rate of gas well production. With the progress of gas well production, the free gas in fracture and matrix system is preferentially produced. The continuous reduction of reservoir pressure makes the gas adsorbed on the surface of organic matter

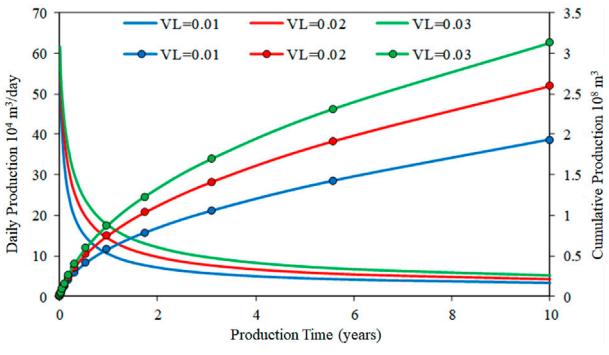

FIGURE 9
Effect of different Langmuir volume on gas well production.

begin to desorption, and enter the fracture system as a reservoir supplementary gas source, delaying the decline of gas well production. When Langmuir volume V_L is 0.01 m^3/kg, 0.02 m^3/kg and 0.03 m^3/kg, the cumulative gas production after 10 years of depletion production is 193 million m^3, 260 million m^3 and 313 million m^3, respectively. Adsorption and desorption is a unique seepage mechanism of shale gas reservoir, which is different from conventional gas reservoir. With the progress of production, the reservoir pressure decreases and the adsorption gas is desorbed in large quantities, which will contribute to the production replenishment and stable production of fractured horizontal wells in shale gas reservoir in the middle and later stages.

6 Conclusion

(1) Simulation studies show that the micro-seismic data and discrete fracture model can be used to reasonably characterize fracture geometry and complex boundary characteristics, and the influence of fracture network on production dynamics can be accurately simulated.
(2) Parameter sensitivity analysis shows that the higher the fracture water saturation, the lower the gas well production; The hydraulic fracture conductivity has obvious influence on the early production of shale gas fractured horizontal wells. Complex fracture network stimulation area is the main contribution area of shale gas well output, the better the stimulation effect, the higher the permeability of the stimulation area, the higher the output of shale gas well. Therefore, the fracturing reconstruction of shale gas wells is mainly to improve the reconstruction degree and increase the reconstruction volume.
(3) For fractured horizontal wells in shale gas reservoirs, with a large amount of free gas produced in fractures and matrix systems, the early high production stage ends, and the adsorbed gas adsorbed on the surface of shale matrix is desorbed due to the reduction of reservoir pressure, which becomes the key to the production replenishment and stable production in the middle and late period. The more desorption gas, the greater the cumulative gas production.

Data availability statement

The raw data supporting the conclusion of this article will be made available by the authors, without undue reservation.

Author contributions

HX: Methodology, Software, Writing–original draft, Investigation. MC: Data curation, Investigation, Resources, Writing–review and editing. CJ: Formal Analysis, Investigation, Writing–review and editing. HZ: Investigation, Resources, Writing–original draft. KW: Conceptualization, Supervision, Validation, Writing–review and editing.

Funding

The authors declare financial support was received for the research, authorship, and/or publication of this article. This study was financially supported by the China Postdoctoral Science Foundation (Grant No. 2022M722638), and the Science and Technology Cooperation Project of the CNPC-SWPU Innovation Alliance (Grant No. 2020CX020202).

Conflict of interest

HX, MC, CJ, and HZ were employed by the company Sichuan Changning Natural Gas Development Co., Ltd. KW was employed by the Development Division of Southwest Oil & Gas Field Company.

Publisher's note

All claims expressed in this article are solely those of the authors and do not necessarily represent those of their affiliated organizations, or those of the publisher, the editors and the reviewers. Any product that may be evaluated in this article, or claim that may be made by its manufacturer, is not guaranteed or endorsed by the publisher.

References

Altwaijri, M., Xia, Z. H., Yu, W., Qu, L. C., Hu, Y. P., Xu, Y. F., et al. (2018). Numerical study of complex fracture geometry effect on two-phase performance of shale-gas wells using the fast EDFM method. *J. Petroleum Sci. Eng.* 164, 603–622. doi:10.1016/j.petrol.2017.12.086

Brown, M., Ozkan, E., Ragahavan, R., and Kazemi, H. (2011). Practical solutions for pressure-transient responses of fractured horizontal wells in unconventional shale reservoirs. *SPE Reserv. Eval. Eng.* 14 (6), 663–676. doi:10.2118/125043-PA

Cai, M. F. (2020). Key theories and technologies for surrounding rock stability and ground control in deep mining. *J. Min. Strata Control Eng.* 2 (3), 033037. doi:10.13532/j.jmsce.cn10-1638/td.20200506.001

Cheng, L. S., Wu, Y. H., Huang, S. J., Fang, S. D., Ma, M., Xue, Y. C., et al. (2020). A comprehensive model for simulating gas flow in shale formation with complex fracture networks and multiple nonlinearities. *J. Petroleum Sci. Eng.* 187, 106817. doi:10.1016/j.petrol.2019.106817

Fan, D., Yao, J., Sun, H., Zeng, H., and Wang, W. (2015). A composite model of hydraulic fractured horizontal well with stimulated reservoir volume in tight oil & gas reservoir. *J. Nat. Gas Sci. Eng.* 24, 115–123. doi:10.1016/j.jngse.2015.03.002

Geiger, S., Roberts, S., Matthai, S. K., Zoppou, C., and Burri, A. (2004). Combining finite element and finite volume methods for efficient multiphase flow simulations in highly heterogeneous and structurally complex geologic media. *Geofluids* 4, 284–299. doi:10.1111/j.1468-8123.2004.00093.x

Geng, L. D., Li, G. S., Tian, S. C., Sheng, M., Ren, W. X., and Zitha, P. (2016). A fractal model for real gas transport in porous shale. *AIChE J.* 63, 1430–1440. doi:10.1002/aic.15516

Guo, W., Zhang, X. W., Yu, R. Z., Kang, L. X., Gao, J. L., and Liu, Y. Y. (2022). A model for the apparent gas permeability of shale matrix organic nanopore considering multiple physical phenomena. *Front. Earth Sci.* 9, 2296–6463. doi:10.3389/feart.2021.813585

Javadpour, F. (2009). Nanopores and apparent permeability of gas flow in mudrocks (shales and siltstone). *J. gas Can. Petroleum Technol.* 48, 16–21. doi:10.2118/09-08-16-DA

Jiang, J. M., and Rami, M. Y. (2015). A multimechanistic multicontinuum model for simulating shale gas reservoir with complex fractured system. *Fuel* 161, 333–344. doi:10.1016/j.fuel.2015.08.069

Karimi-Fard, M., Durlofsky, L. J., and Aziz, K. (2004). An efficient discrete-fracture model applicable for general-purpose reservoir simulators. *SPE J.* 9, 227–236. doi:10.2118/88812-PA

Li, H. (2023). Coordinated development of shale gas benefit exploitation and ecological environmental conservation in China: A mini review. *Front. Ecol. Evol.* 11, 1232395. doi:10.3389/fevo.2023.1232395

Li, H. T., Wang, J. C., Li, Y., and Luo, W. (2015). Deliverability evaluation method based on volume source for horizontal wells by staged fracturing. *Nat. Gas. Ind.* 35, 55–63. doi:10.3787/j.issn.1000-0976.2015.09.008

Li, J., Li, H., Yang, C., Ren, X. H., and Li, Y. D. (2023). Geological characteristics of deep shale gas and their effects on shale fracability in the Wufeng–Longmaxi Formations of the southern Sichuan Basin, China. *Lithosphere* 2023 (1), 4936993. doi:10.2113/2023/4936993

Liu, Y. W., Gao, D. P., Li, Q., Wan, Y. Z., Duan, W. J., Zeng, X. G., et al. (2019). Mechanical frontiers in shale-gas development. *Adv. Mech.* 49 (1), 201901. doi:10.6052/1000-0992-17-020

Lv, X. R., Yao, J., Huang, Z. Q., and Zhao, J. (2012). Study on discrete fracture model two-phase flow simulation based on finite volume method. *J. Southwest Petroleum University:Science Technol. Ed.* 34, 123–130. doi:10.3863/j.issn.1674-5086.2012.06.018

Moinfar, A., Varavei, A., Sepehrnoori, K., and Johns, R. T. (2013). *Development of a coupled dual continuum and discrete fracture model for the simulation of unconventional reservoirs*. The Woodlands, TX, USA: Study SPE 163647 presented at the SPE Reservoir Simulation Symposium.

Ozkan, E., Brown, M., Raghavan, R., and Kazemi, H. (2011). Comparison of fractured-horizontal-well performance in tight sand and shale reservoirs. *SPE Reserv. Eval. &Engineering* 14 (02), 248–259. doi:10.2118/121290-PA

Stalgorova, E., and Mattar, L. (2013). Analytical model for unconventional multifractured composite systems. *SPE Reserv. Eval. Eng.* 16, 246–256. doi:10.2118/162516-PA

Sun, Z. M. (2023). Superimposed hydrocarbon accumulation through multi-source and multi-stage evolution in the cambrian xixiangchi group of eastern sichuan basin: A case study of the pingqiao gas-bearing anticline. *Energy Geosci.* 4 (1), 131–142. doi:10.1016/j.engeos.2022.09.001

Wang, H. T. (2014). Performance of multiple fractured horizontal wells in shale gas reservoirs with consideration of multiple mechanisms. *J. Hydrology* 510, 299–312. doi:10.1016/j.jhydrol.2013.12.019

Wang, X. C., Rasouli, V., Damjanac, B., Yu, W., Xie, H. B., Li, N., et al. (2020). Coupling of fracture model with reservoir simulation to simulate shale gas production with complex fractures and nanopores. *J. Petroleum Sci. Eng.* 193, 107422. doi:10.1016/j.petrol.2020.107422107422

Wu, K. L., Li, X. F., and Chen, Z. X. (2016). Micro-scale effects of gas transport in organic nanopores of shale gas reservoirs. *Nat. Gas. Ind.* 36, 51–64. doi:10.3787/j.issn.1000-0976.2016.11.007

Wu, K. (2014). *Numerical modeling of complex hydraulic fracture development in unconventional reservoirs*. Austin, TX, USA: The University of Texas at Austin.

Wu, Y. S., and Pruess, K. A. (1988). A multiple-porosity method for simulation of naturally fractured Petroleum reservoirs. *SPE Reserv. Eval. Eng.* 3, 327–336. doi:10.2118/15129-PA

Wu, Z. W., Cui, C. Z., Jia, P. F., Wang, Z., and Sui, Y. F. (2022). Advances and challenges in hydraulic fracturing of tight reservoirs: A critical review. *Energy Geosci.* 3 (4), 427–435. doi:10.1016/j.engeos.2021.08.002

Xie, J. (2018). Practices and achievements of the Changning-Weiyuan shale gas national demonstration project construction. *Nat. Gas. Ind.* 38, 1–7. doi:10.3787/j.issn.1000-0976.2018.02.001

Xu, J. C., Guo, C. H., Wei, M. Z., and Jiang, R. Z. (2015). Production performance analysis for composite shale gas reservoir considering multiple transport mechanisms. *J. Nat. Gas Sci. Eng.* 26, 382–395. doi:10.1016/j.jngse.2015.05.033

Yang, Z. H., Hu, Z. Q., Xiong, L., Ding, J. H., Shen, B. J., Shi, H. L., et al. (2020). Gas storage characteristics and coupling characteristics of deep shale gas: A case study of well-X in southern sichuan basin, China. *Reserv. Eval. Dev.* 10, 20–27. doi:10.13809/j.cnki.cn32-1825/te.2020.05.003

Yuan, B., Su, Y. L., Moghanloo, R. G., Rui, Z. H., Wang, W. D., and Shang, Y. Y. (2015). A new analytical multi-linear solution for gas flow toward fractured horizontal wells with different fracture intensity. *J. Nat. Gas Sci. Eng.* 23, 227–238. doi:10.1016/j.jngse.2015.01.045

Zhu, Q. Y., Dai, J., Yun, F. F., Zhai, H. H., Zhang, M., and Feng, L. R. (2022). Dynamic response and fracture characteristics of granite under microwave irradiation. *J. Min. Strata Control. Eng.* 4 (1). doi:10.13532/j.jmsce.cn10-1638/td.20210926.001019921

Zhang, D. L., Zhang, L. H., Zhao, Y. L., and Guo, J. J. (2015). A composite model to analyze the decline performance of a multiple fractured horizontal well in shale reservoirs. *J. Nat. Gas Sci. Eng.* 26, 999–1010. doi:10.1016/j.jngse.2015.07.034

Zhang, L. H., Jia, M., Zhang, R. H., and Guo, J. J. (2017). Discrete fracture network modeling and numerical simulation of fractured reservoirs. *J. Southwest Petroleum University:Science Technol. Ed.* 39, 121–127. doi:10.11885/j.issn.1674-5086.2016.03.31.03

Zhang, R. H., Chen, M., Tang, H. Y., Xiao, H. S., and Zhang, D. L. (2023). Production performance simulation of a horizontal well in a shale gas reservoir considering the propagation of hydraulic fractures. *Geoenergy Sci. Eng.* 221, 111272doi:10.1016/j.petrol.2022.111272

Zhang, T., Li, X. F., Wang, X. Z., Li, J., Sun, Z., Feng, D., et al. (2018). A discrete model for apparent gas permeability in nanoporous shale coupling initial water distribution. *J. Nat. Gas Sci. Eng.* 59, 80–96. doi:10.1016/j.jngse.2018.08.024

Zhao, J. Z., Ren, L., Shen, C., and Li, Y. M. (2018a). Latest research progresses in network fracturing theories and technologies for shale gas reservoirs. *Nat. Gas. Ind.* 38, 533–546. doi:10.1016/j.ngib.2018.03.007

Zhao, Y. L., Zhang, L. H., and Shan, B. C. (2018b). Mathematical model of fractured horizontal well in shale gas reservoir with rectangular stimulated reservoir volume. *J. Nat. Gas Sci. Eng.* 59, 67–79. doi:10.1016/j.jngse.2018.08.018

Zou, C. N., Guo, J. L., Jia, A. L., Wei, Y. S., Yan, H. J., Jia, C. Y., et al. (2020). Connotation of scientific development for giant gas fields in China. *Nat. Gas. Ind.* 40, 1–12. doi:10.3787/j.issn.1000-0976.2020.03.001